


Article

Electromechanical Actuator Servo Control Technology Based on Active Disturbance Rejection Control

Qian Fang ¹, Yong Zhou ^{1,*}, Shangjun Ma ², Chao Zhang ¹, Ye Wang ¹ and Haibin Huangfu ¹¹ School of Aeronautics, Northwestern Polytechnical University, Xi'an 710072, China² School of Mechanical Engineering, Northwestern Polytechnical University, Xi'an 710072, China

* Correspondence: yongstar@nwpu.edu.cn; Tel.: +86-133-7928-2465

Abstract: Electromechanical actuators (EMA) are becoming more and more widely used. As the core technology of EMA, servo control technology determines their performance. In this paper, an active disturbance rejection control (ADRC) method with an improved extended state observer (ESO) is proposed to design a cascade controller of EMA based on permanent magnet synchronous motor (PMSM). The mathematical model of PMSM in a two-phase rotating coordinate system is established, then it is decoupled by an $i_d = 0$ current control method to realize the vector control of the motor. In a three closed-loop vector control system, a PID controller including current loop, speed loop and position loop is designed. To solve the problems caused by measurement noise, the filter link and system are modeled as a whole, and an improved ESO is constructed. On this basis, an ADRC controller of the speed loop and position loop of PMSM is designed and simulated based on Simulink. Based on the physical test platform, a load step test and load disturbance test of ADRC are completed. The results show that, in comparison to the PID method, the ADRC method shortens the response time by 25% on average, and reduces the overshoot by 60% on average. So, it can be concluded that ADRC has good static and dynamic performance, which has a good guiding role for engineering practice.

Keywords: EMA; PMSM; ADRC; ESO

Citation: Fang, Q.; Zhou, Y.; Ma, S.; Zhang, C.; Wang, Y.; Huangfu, H. Electromechanical Actuator Servo Control Technology Based on Active Disturbance Rejection Control. *Electronics* **2023**, *12*, 1934. <https://doi.org/10.3390/electronics12081934>

Academic Editors: Teng Zhou and Liang Yan

Received: 27 February 2023

Revised: 16 April 2023

Accepted: 17 April 2023

Published: 19 April 2023



Copyright: © 2023 by the authors. Licensee MDPI, Basel, Switzerland. This article is an open access article distributed under the terms and conditions of the Creative Commons Attribution (CC BY) license (<https://creativecommons.org/licenses/by/4.0/>).

1. Introduction

With the continuous development of science and technology, there are also new requirements for modern aircraft. Faster speed, better maneuverability and lighter weight are required. The improvement of these aspects is also a new challenge for the performance of its control system. There are higher requirements of the rapidity, accuracy, stability and robustness of the control system. As the executive mechanism of the control system, the servo actuator directly determines the performance of the control attitude of the aircraft.

During pitch, roll and yaw maneuvers, the servo actuator controls the rudder surface, thereby influencing the control performance of the aircraft. Servo actuators can be classified into two distinct types based on their structures, namely Electrohydraulic actuators (EHA) and Electromechanical actuators (EMA). Compared with EHA, EMA completely cancel the hydraulic component and replace the rigid oil pipeline with flexible cable, which improves the portability and reliability of the actuator. EMA use the mechanical transmission mechanism driven by the motor to control the movement of the actuating cylinder, which makes the response faster and more accurate, and further improves the actuating efficiency. In the foreseeable future, a large number of EMA will be used in modern aircraft to realize full electrification and digitalization [1–5].

EMA based on permanent magnet synchronous motor (PMSM) possess advantages of structural reliability and high control accuracy, which are commonly used in high-precision servo systems. Common servo control technologies include PID control, fuzzy control, sliding mode variable structure control, model predictive control, adaptive control, neural

network control, active disturbance rejection control (ADRC), etc. PID control is a conventional linear control strategy that has a good computational capability. However, it faces difficulty in achieving the control requirements of a motor when dealing with nonlinear controlled objects and complex systems. Sliding mode variable structure control has advantages in terms of its good dynamic characteristics and robustness, but its downside is the chattering problem caused by the system oscillating around the balancing point. Adaptive control exhibits good robustness and dynamic performance in the control of PMSM and overcomes the influences of various disturbances, but it changes the control performance indicator according to the feedback information, resulting in a slow operation speed, a long time being taken for online identification and calibration, and a lack of rapid motor control. Fuzzy control is suitable for controlling nonlinear time-varying systems, but it reduces the accuracy of system control due to the foggy handling of information. Additionally, it is difficult for fuzzy control to eliminate steady-state errors, making it unable to achieve precise control of PMSM [6–9].

The ADRC method consists of a tracking differentiator, an extended state observer (ESO) and a nonlinear error feedback controller. The tracking differentiator is responsible for arranging the transition process and extracting the differential signal of the control objective to resolve the contradiction between system overshoot and quickness. The ESO is responsible for observing the state of the controlled object and the internal and external disturbances in the object model. The nonlinear error feedback controller compensates for the internal and external disturbances of the object model, transforming the system into an integral concatenation type system and achieving feedback linearization of the dynamic system [10–13]. Reference [14] proposed an Improved Active Disturbance Rejection Control (I-ADRC) method to enhance the disturbance attenuation of the speed controller for PMSM. The results showed that the proposed controller had less steady-state errors and a stronger disturbance attenuation ability than the PID controller. Reference [15] proposed an Adaptive ADRC strategy for sensorless induction motor drives, which demonstrated a good control performance of ADRC in the absence of speed sensors. Reference [16] discusses the actual application of ADRC in induction motors, and the results show that ADRC can reduce the impact of unmodeled dynamics and external disturbances. Reference [17] optimizes traditional cascaded vector control and constructs a rotor flux control loop and a speed control loop based on ADRC, estimating and compensating for internal and external disturbances using two linear ESOs. Reference [18] designs a linear ADRC for a single-winding, bearingless flux-switching permanent magnet motor based on model compensation, constructing a linear extended state observer and linear feedback control law with known model disturbance information, and proposes a corresponding parameter selection strategy. Compared with PID control, it has a stronger anti-interference ability under the same stability margin. The ADRC method simplifies the complex model through the ESO and optimizes the simplified system for achieving the combination of dynamic response and disturbance rejection ability [19,20]. Therefore, it is well suited for application in EMA based on PMSM.

This paper initially establishes the mathematical model of PMSM, and subsequently employs $i_d = 0$ current control method to achieve decoupling between the d axis and q axis. It also develops a three closed-loop PID controller for position control. Additionally, an ADRC method based on an improved observer is proposed to achieve the stable control of PMSM. Experiments are conducted on a test platform and the results are analyzed. Finally, the paper summarizes the work done and proposes areas for improvement.

2. Materials and Methods

2.1. Control of PMSM

2.1.1. Mathematical Model of PMSM

The mathematical model of PMSM includes four equations: voltage equation, flux linkage equation, torque equation and motion equation. Because PMSM does not include

rotor winding, the voltage equation and flux linkage equation only need to be written in the stator side equation.

From the mechanical structure of PMSM, the mathematical model in a three-phase static (ABC) coordinate system could be obtained. Based on the principle that the synthesized magnetomotive force generated by the winding is equivalent, the mathematical model in a two-phase rotating (dq) coordinate system could be simplified as follows:

1. Stator voltage equation The stator voltage equation in dq coordinate system is

$$\begin{cases} u_d = R_s i_d + \frac{d\psi_d}{dt} - \omega_e \psi_q \\ u_q = R_s i_q + \frac{d\psi_q}{dt} + \omega_e \psi_d \end{cases} \quad (1)$$

In the equation: u_d and u_q are stator voltage component in dq coordinate system; R_s is per phase resistance of three-phase symmetrical stator winding; i_d and i_q are stator current component in dq coordinate system; ψ_d and ψ_q are flux linkage component in dq coordinate system; ω_e is the electrical angular velocity of rotor rotation.

2. Stator flux linkage equation The stator flux linkage equation in dq coordinate system is

$$\begin{cases} \psi_d = \psi_f + L_d i_d \\ \psi_q = L_q i_q \end{cases} \quad (2)$$

In the equation: ψ_f is the flux linkage generated for permanent magnets; L_d and L_q are the inductance of the orthogonal and direct axis in dq coordinate system.

3. Electromagnetic torque equation The electromagnetic torque equation in dq coordinate system is

$$T_e = 1.5n_p(\psi_d i_q - \psi_q i_d) \quad (3)$$

In the equation: T_e is the electromagnetic torque of PMSM; n_p is pole pairs of the rotor.

4. Motion equilibrium equation The equation of motion in dq coordinate system remains unchanged, which is

$$T_e = \frac{J}{n_p} \frac{d\omega_e}{dt} + T_l \quad (4)$$

In the equation: T_l is the load torque.

2.1.2. Vector Control Technology

Of the two main control methods of PMSM, vector control and direct torque control, vector control technology is the most widely used at present. The current control methods commonly used in vector control technology are: $i_d = 0$ control, MTPA control, $\cos \varphi = 1$ control and constant flux control. Different control methods will lead to different operating efficiency, power factor and torque of the motor.

The $i_d = 0$ control method employs decoupling control of the d and q axis current to maintain the direct-axis current component at zero and ensure that the armature reaction has no direct-axis electromagnetic component, thus avoiding demagnetization effects. This makes the electromagnetic torque proportional to the stator current, and guarantees that the stator magnetomotive force space vector and rotor magnetic field space vector are orthogonal. In this study, since the focus is on a low-power and high-performance servo system, the $i_d = 0$ control method is chosen.

In the case of adopting $i_d = 0$ control, the mathematical model of PMSM in dq coordinate system could be simplified. Equation (1) can be written as follows

$$\begin{cases} u_d = -\omega_e L_q i_q \\ u_q = R_s i_q + L_q \frac{di_q}{dt} + \omega_e \psi_f \end{cases} \quad (5)$$

Equation (3) can be written as follows

$$T_e = 1.5n_p\psi_f i_q \tag{6}$$

Substitute $\omega_e = n_p\omega_m$ into Equation (5), ω_m is the mechanical angular velocity, and it can be obtained that

$$u_q = R_s i_q + L_q \frac{di_q}{dt} + n_p\omega_m\psi_f \tag{7}$$

Carry out Laplace transform on Equation (7), that is

$$\frac{I_q(s)}{U_q(s) - K_e\omega_m(s)} = \frac{1}{L_q s + R} \tag{8}$$

In the equation: $K_e = n_p\psi_f$ is the back emf coefficient. Substitute Equation (6) into Equation (4), that is

$$1.5n_p\psi_f i_q = T_l + J \frac{d\omega_m}{dt} \tag{9}$$

Make a Laplace transform of Equation (9), that is

$$\frac{\omega_m(s)}{K_t I_q(s) - T_l(s)} = \frac{1}{Js} \tag{10}$$

In the equation: $K_t = 1.5n_p\psi_f$, is the torque coefficient.

The structural block diagram of PMSM can be obtained from Equations (8) and (10), as shown in Figure 1. It can be seen that $i_d = 0$ control completely decouples the quadrature-axis and direct-axis of PMSM, and the speed control and torque control are only related to the q axis current, which greatly simplifies the model of PMSM and achieves the control effect comparable to that of the DC motor.

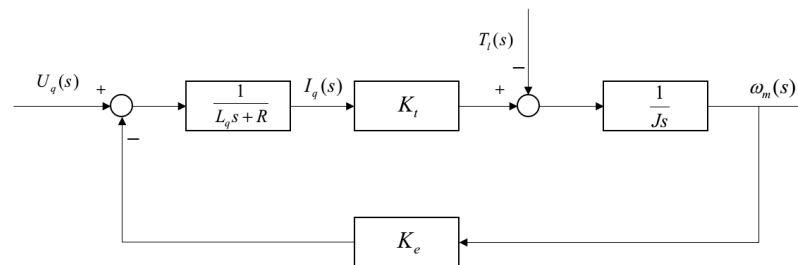


Figure 1. PMSM Dynamic Structure Diagram.

According to the decoupled PMSM model, the common position vector control flow chart is shown in Figure 2.

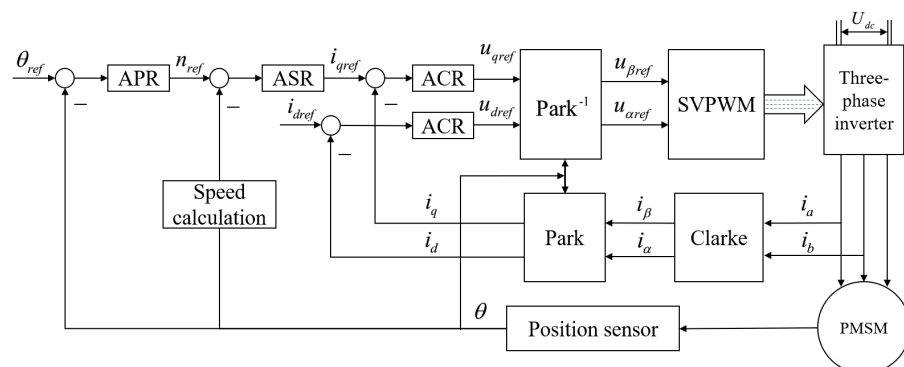


Figure 2. Position Vector Control Flow Chart.

As can be seen from Figure 2, the commonly used position vector control system adopts a three closed-loop control structure, including position loop, speed loop and current loop from outside to inside. APR is the position regulator, ASR is the speed regulator and ACR is the current regulator. The position loop receives the given position command and makes the difference with the feedback value measured by the position sensor, and the obtained result is the given value of the position regulator. The speed command is then calculated by the position regulator. The speed loop receives the speed instruction given by the position loop and makes the difference with the speed signal obtained by differentiating the position signal. The obtained result is the given value of the speed regulator and the q axis current instruction is calculated by the speed regulator. In the current loop, the given value of the d axis current is always zero. The q axis current loop receives the current instruction given by the speed loop and, after making the difference with the current feedback value, the given value of the d and q axis voltage are calculated by the current regulator, and the d and q axis voltage are transformed by Park⁻¹ to obtain the voltage value u_α and u_β in a two-phase stationary ($\alpha\beta$) coordinate system. The PWM waveform is generated through the space vector pulse width modulation (SVPWM) technology, and the voltage vector of the motor is controlled by the inverter to complete the position vector control of PMSM.

2.1.3. Three Closed-Loop Controller Design

1. Current loop design

As can be seen from Figure 1, the back electromotive force of the motor affects the design of the current loop. In fact, the speed change of the motor is much slower than its current change, so the influence of back electromotive force on the current loop can be ignored. The structure diagram of the current loop is shown in Figure 3.

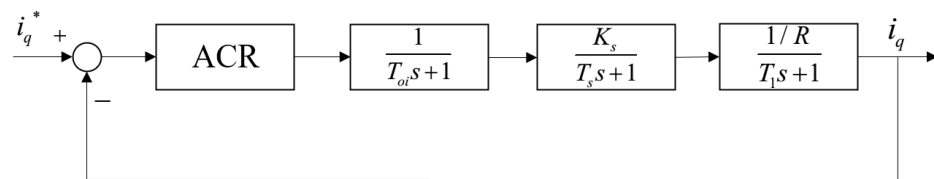


Figure 3. Structure Diagram of the Current Loop.

In the diagram: $\frac{1}{T_{oi}s+1}$ is the inertia link of the equivalent filter; $\frac{K_s}{T_s s+1}$ is the inertia link of equivalent inverter; K_s is the amplification factor of the inverter; T_s is the time constant of the inverter; T_{oi} is the time constant of the filter; $T_1 = \frac{L_q}{R}$.

Because the time constant T_{oi} and T_s are far less than T_1 , the current loop structure can be approximated as shown in Figure 4. In the figure, $T_{\Sigma i} = T_{oi} + T_s$.

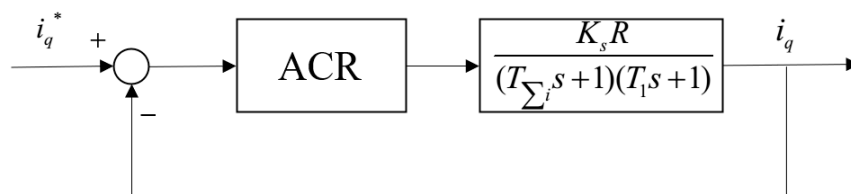


Figure 4. Equivalent Structure Diagram of the Current Loop.

The performance requirement of current loop are fast tracking and no static error in steady state, so the current loop is designed as I-type system. The current regulator uses the classic PI regulator, and its transfer function is

$$W_{ACR}(s) = K_{pACR} \frac{\tau_{ACR}s + 1}{\tau_{ACR}s} \tag{11}$$

Because T_1 is much larger than $T_{\Sigma i}$, taking $\tau_{ACR} = T_1$ can realize the cancellation of the zero point of the current regulator and the system dominant pole. Figure 4 can be simplified to the structure shown in Figure 5.

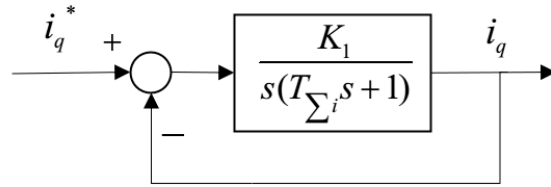


Figure 5. Simplified Structure Diagram of the Current Loop.

In the figure: $K_1 = K_{pACR} \frac{K_s/R}{\tau_{ACR}}$.

At this time, the closed-loop transfer function of the current loop is

$$G_{ci}(s) = \frac{G_{oi}(s)}{G_{oi}(s) + 1} = \frac{1}{\frac{T_{\Sigma i}}{K_1}s^2 + \frac{1}{K_1}s + 1} \tag{12}$$

This system is a typical second-order system. According to the engineering design method, the damping ratio is set to 0.707, and then $K_1 T_{\Sigma i} = 0.5$. The proportional coefficient of current regulator is

$$K_{pACR} = \frac{L_q}{2K_s T_{\Sigma i}} \tag{13}$$

2. Speed loop design

In the design of speed loop, the current loop is approximately an inertial link,

$$W_{cli}(s) = \frac{1}{\frac{1}{K_1}s + 1} = \frac{1}{2T_{\Sigma i}s + 1} \tag{14}$$

Substituting the equivalent link of the current loop obtained by Equation (14) into the speed loop, the structure diagram of the speed loop as shown in Figure 6 can be obtained.

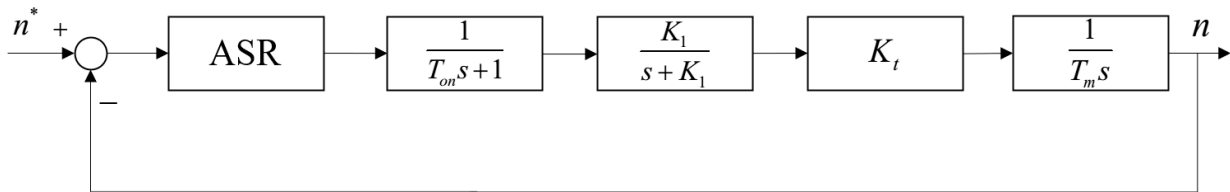


Figure 6. Structure Diagram of the Speed Loop.

In the figure: $\frac{1}{T_{on}s + 1}$ is the inertia link of the equivalent filter; T_{on} is the time constant of the filter; $T_m = J \frac{2\pi}{60}$.

The two inertial links in Figure 6 can be approximated as one inertial link, and the structure diagram of the speed loop as shown in Figure 7 can be obtained. In the figure $T_{\Sigma n} = T_{on} + 2T_{\Sigma i}$.

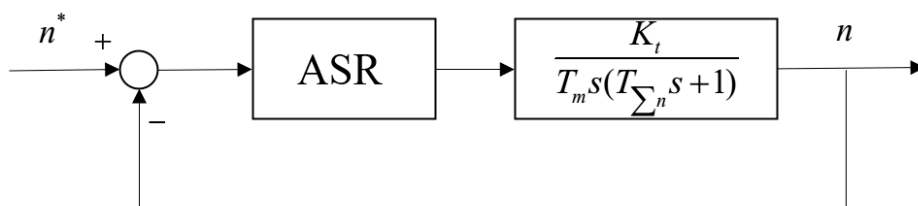


Figure 7. Equivalent Structure Diagram of the Speed Loop.

The performance requirement of the speed loop is no static errors, and it has a good ability to suppress disturbance, so the speed loop is designed as an II-type system. Its structural diagram is shown in Figure 8. The speed loop also adopts a PI regulator, and its transfer function is

$$W_{ASR}(s) = K_{pASR} \frac{\tau_{ASR}s + 1}{\tau_{ASR}s} \tag{15}$$

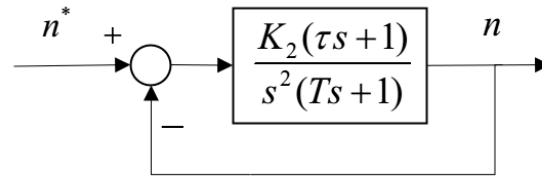


Figure 8. Equivalent Structure Diagram-2 of the Speed Loop.

According to the undetermined coefficient method, there is $K_2 = \frac{K_{pASR} K_t}{\tau_{ASR} T_m}$, $\tau = \tau_{ASR}$, $T = T_{\Sigma n}$.

According to the engineering design method, the medium bandwidth is usually taken, that is $h = 5$. The time constant of the speed regulator can be obtained: $\tau_{ASR} = 5T_{\Sigma n}$.

According to the criterion for minimizing the peak value of closed-loop amplitude-frequency characteristics, we can get

$$K_2 = \frac{h + 1}{2h^2 T^2} \tag{16}$$

The proportional coefficient of the speed loop regulator is

$$K_{pASR} = \frac{\tau_{ASR} T_m (h + 1)}{2h^2 T_{\Sigma n}^2 K_t} \tag{17}$$

The cut-off frequency of the speed loop is

$$\omega_n = K_2 \tau = 2.5 \frac{h + 1}{h^2 T_{\Sigma n}} \tag{18}$$

3. Position loop design

In the design of the position loop, the velocity loop is approximated as an inertial link.

$$W_{cIn}(s) = \frac{1}{T_n s + 1} \tag{19}$$

In the equation: $T_n \omega_n = 1$.

The equivalent link of the speed loop obtained by Equation (17) is substituted into the position loop, and because the performance requirement of the position loop is no overshoot, P regulator is selected. The position loop structure diagram is used, as shown in Figure 9.

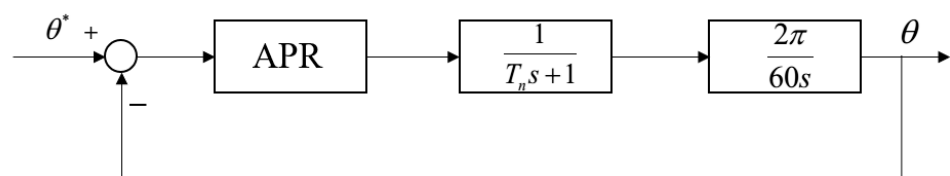


Figure 9. Structure Diagram of the Position Loop.

The system is a typical I-type system. According to the engineering design method, the damping ratio is 1.0. At this time, there are

$$K_{pAPR}T_n \cdot \frac{2\pi}{60} = 0.25 \tag{20}$$

The proportional coefficient of the position regulator is

$$K_{pAPR} = \frac{15}{2\pi T_n} \tag{21}$$

2.2. Linear ADRC

There are three components of nonlinear ADRC, a tracking differentiator, ESO and error feedback control law, which all adopt nonlinear functions. Although the nonlinear function can achieve a better control effect, it has many parameters and is very troublesome to set. Research found that the performance of ADRC constructed by linear function is similar to that of nonlinear ADRC, and there are less parameters and they are easy to adjust. Considering the perfect configuration of the transition process in the industrial field, the linear active disturbance rejection controller cancels the tracking differentiator, and consists of a linear ESO and a linear error feedback control law.

2.2.1. Improved ESO

The linear ESO adopts the structure of a full-dimensional observer, and does not consider the influence of measurement noise on the system. In practical application, the filter can be equivalent to the form of inertial link. Here, the actual system and inertial link are combined, and an ESO is constructed for the combined system to solve the problems caused by the introduction of the filter [21–25].

Existing first-order system

$$\dot{y} = f(y, w, t) + bu \tag{22}$$

Select the state variable $x_1 = y, x_2 = f(y, w, t)$, and write the state equation as

$$\begin{cases} \dot{x}_1 = x_2 + bu \\ \dot{x}_2 = f \\ y = x_1 \end{cases} \tag{23}$$

The filter is equivalent to a first-order inertial link, and its expression is

$$\dot{y}_0 = -ay_0 + ay \tag{24}$$

In the equation: y_0 is output signal of the filter; a is the reciprocal of the time constant of inertia link.

The output signal of the extended filter is a new state variable x_0 , and the state equation of the combined system is

$$\begin{cases} \dot{\mathbf{x}} = \mathbf{A}\mathbf{x} + \mathbf{B}u + \mathbf{E}\dot{f} \\ y = \mathbf{C}\mathbf{x} \end{cases} \tag{25}$$

In the equation: $A = \begin{bmatrix} -a & a & 0 \\ 0 & 0 & 1 \\ 0 & 0 & 0 \end{bmatrix}, B = \begin{bmatrix} 0 \\ b \\ 0 \end{bmatrix}, E = \begin{bmatrix} 0 \\ 0 \\ 1 \end{bmatrix}, \mathbf{x} = \begin{bmatrix} x_0 \\ x_1 \\ x_2 \end{bmatrix}, C = [1 \ 0 \ 0]$.

The linear state observer is constructed for this system. There is

$$\begin{cases} \dot{\mathbf{z}} = [\mathbf{A} - \mathbf{L}\mathbf{C}]\mathbf{z} + [\mathbf{B}, \mathbf{L}]\mathbf{u}_c \\ \mathbf{y}_c = \mathbf{z} \end{cases} \tag{26}$$

Using the pole assignment method, the pole is assigned at $-\omega_o$, and the solution is

$$L = \left[3\omega_o - a \quad \frac{3\omega_o^2}{a} \quad \frac{\omega_o^3}{a} \right]^T \quad (27)$$

The condition that enables the full-dimensional observer to configure any pole is that the system can be observed. So, it is necessary to verify whether the system in Equation (25) can be observed.

According to the criterion of system observability, if $a \neq 0$, there is

$$\text{rank} \begin{bmatrix} C \\ CA \\ CA^2 \end{bmatrix} = \text{rank} \begin{bmatrix} 1 & 0 & 0 \\ -a & a & 0 \\ a^2 & -a^2 & a \end{bmatrix} \equiv 3 \quad (28)$$

Therefore, the system can be completely observed and can be arbitrarily configured.

The improved ESO retains the advantages of linear ESO, with only one adjustment parameter and simple tuning. At the same time, the influence of filter introduction on the system is solved by introducing a new extended state. Time-delay systems are often treated as inertial links, and the improved ESO can also improve the time delay of the system.

2.2.2. Linear Error Feedback Control Law

The linear ADRC adopts linear PD feedback control law. For the compensated second-order series integration system $\dot{y} = u_0$, the common PD feedback control law is

$$u_0 = k_p(v - z_1) - k_d z_2 \quad (29)$$

In the equation: v is the target value; z_1 and z_2 are the observation value output by the observer; k_p and k_d are the proportional coefficient and differential coefficient. The differential term of the target value is omitted in the equation to avoid the oscillation caused by it.

The closed-loop transfer function of the system using Equation (29) is

$$G_{cl} = \frac{k_p}{s^2 + k_d s + k_p} \quad (30)$$

The poles of the system in Equation (30) are assigned at $-\omega_c$, ω_c is the bandwidth of the controller, then

$$\begin{cases} k_p = \omega_c^2 \\ k_d = 2\omega_c \end{cases} \quad (31)$$

To sum up, the linear error feedback law links the controller parameters with the bandwidth, and the adjustable parameters are reduced to one, which facilitates the parameter tuning of the controller.

2.3. Design of Linear Active Disturbance Rejection Controller for PMSM

By combining the linear ESO with the linear error feedback control law, a linear ADRC controller has been obtained. For example, taking the second-order system in Equation (23), the structure of the linear ADRC controller is shown in Figure 10.

After adopting current closed-loop control, the mathematical model of PMSM is

$$\begin{cases} \dot{\theta}_m = \omega_m \\ \omega_m = \frac{n_p^2 \psi_f}{J} i_q - \frac{T_l}{J} \end{cases} \quad (32)$$

According to Equation (28), the ADRC controller of the speed loop and position loop of PMSM is designed.

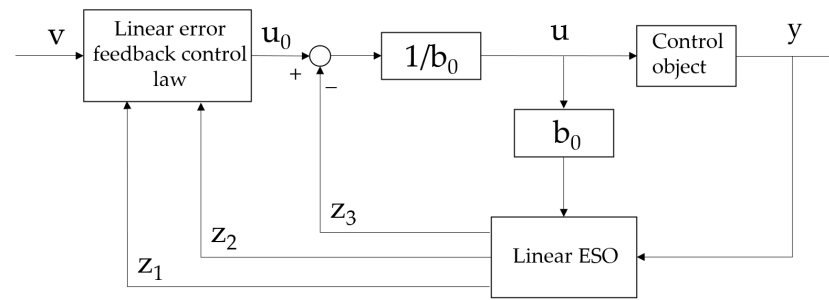


Figure 10. Structure Diagram of the Linear ADRC controller.

2.3.1. Design of Active Disturbance Rejection Controller for the Speed Loop

The system expression of the speed loop is

$$\omega_m = \frac{n_p^2 \psi_f}{J} i_q - \frac{T_l}{J} \tag{33}$$

Assume $x_1 = \omega$, $x_2 = -\frac{T_l}{J} = f$, $b = \frac{n_p^2 \psi_f}{J}$, $u = i_q$, and the time constant of inertia link is a_1 . The linear ESO is constructed as

$$\begin{cases} \dot{z}_0 = -3\omega_0 z_0 + a_1 z_1 + (3\omega_0 - a_1)y \\ \dot{z}_1 = -\frac{3\omega_0^2}{a_1} z_0 + z_2 + bu + \frac{3\omega_0^2}{a_1} y \\ \dot{z}_2 = -\frac{\omega_0^3}{a_1} z_0 + \frac{\omega_0^3}{a_1} y \\ \mathbf{y}_c = \mathbf{z} \end{cases} \tag{34}$$

Proportional feedback is adopted, and the ADRC of speed loop is

$$\begin{cases} \dot{z}_0 = -3\omega_0 z_0 + a_1 z_1 + (3\omega_0 - a_1)y \\ \dot{z}_1 = -\frac{3\omega_0^2}{a_1} z_0 + z_2 + bu + \frac{3\omega_0^2}{a_1} y \\ \dot{z}_2 = -\frac{\omega_0^3}{a_1} z_0 + \frac{\omega_0^3}{a_1} y \\ u_0 = k_p(v - z_1) \\ u = \frac{u_0 - z_2}{b} \end{cases} \tag{35}$$

2.3.2. Design of the Position Loop ADRC

The system expression of the position loop is

$$\dot{\theta}_m = \omega_m \tag{36}$$

Assume $x_1 = \theta_m$, x_2 is an unknown disturbance, $b = 1$, $u = \omega_m$ and the time constant of inertia link is a_2 , and the linear ESO is constructed as

$$\begin{cases} \dot{z}_0 = -3\omega_0 z_0 + a_2 z_1 + (3\omega_0 - a_2)y \\ \dot{z}_1 = -\frac{3\omega_0^2}{a_2} z_0 + z_2 + bu + \frac{3\omega_0^2}{a_2} y \\ \dot{z}_2 = -\frac{\omega_0^3}{a_2} z_0 + \frac{\omega_0^3}{a_2} y \\ \mathbf{y}_c = \mathbf{z} \end{cases} \tag{37}$$

Adopting proportional feedback, the position loop ADRC is

$$\begin{cases} \dot{z}_0 = -3\omega_0 z_0 + a_2 z_1 + (3\omega_0 - a_2)y \\ \dot{z}_1 = -\frac{3\omega_0^2}{a_2} z_0 + z_2 + bu + \frac{3\omega_0^2}{a_2} y \\ \dot{z}_2 = -\frac{\omega_0^3}{a_2} z_0 + \frac{\omega_0^3}{a_2} y \\ u_0 = k_p(v - z_1) \\ u = \frac{u_0 - z_2}{b} \end{cases} \tag{38}$$

2.3.3. Stability Analysis of ADRC

Arranging Equation (35) could get

$$\begin{bmatrix} \dot{z}_0 \\ \dot{z}_1 \\ \dot{z}_2 \end{bmatrix} = \begin{bmatrix} -3\omega_0 & a_1 & 0 \\ -\frac{3\omega_0^2}{a_1} & 0 & 1 \\ -\frac{\omega_0^3}{a_1} & 0 & 0 \end{bmatrix} \begin{bmatrix} z_0 \\ z_1 \\ z_2 \end{bmatrix} + \begin{bmatrix} -3\omega_0 \\ -\frac{3\omega_0^2}{a_1} \\ -\frac{\omega_0^3}{a_1} \end{bmatrix} y + \begin{bmatrix} 0 \\ b \\ 0 \end{bmatrix} u \quad (39)$$

According to the Space State Representation Method in Modern Control Theory, it is easy to know that the expression of coefficient matrix A is

$$A = \begin{bmatrix} -3\omega_0 & a_1 & 0 \\ -\frac{3\omega_0^2}{a_1} & 0 & 1 \\ -\frac{\omega_0^3}{a_1} & 0 & 0 \end{bmatrix} \quad (40)$$

According to the relationship between the state space equation and the transfer function, it can be known that if the determinant of $sI - A$ is 0, the pole equation of the system can be obtained

$$|sI - A| = \begin{vmatrix} s + 3\omega_0 & -a_1 & 0 \\ \frac{3\omega_0^2}{a_1} & s & -1 \\ \frac{\omega_0^3}{a_1} & 0 & s \end{vmatrix} = 0 \quad (41)$$

Then the pole equation of the system can be obtained, s is the eigenvalue of A and the pole of system, and the triple pole $s = -\omega_0$ can be obtained by solving the equation. So, when the pole is assigned at $-\omega_0$, the system is stable. In an improved ESO, when the pole has been assigned at $-\omega_0$, it could concluded that the system is stable.

2.4. Simulation of the Linear ADRC System for PMSM

Based on Simulink, the design of the ADRC system is modeled and simulated. Its speed loop is shown in Figure 11 and its speed step response is shown in Figure 12.

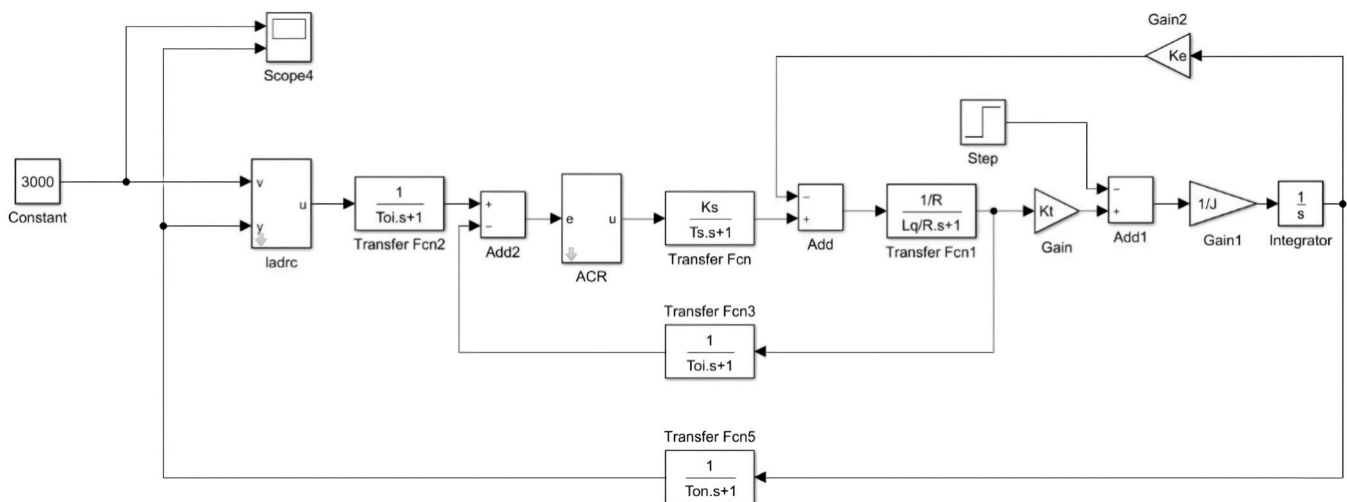


Figure 11. Structure Diagram of the ADRC Speed Loop Simulation.

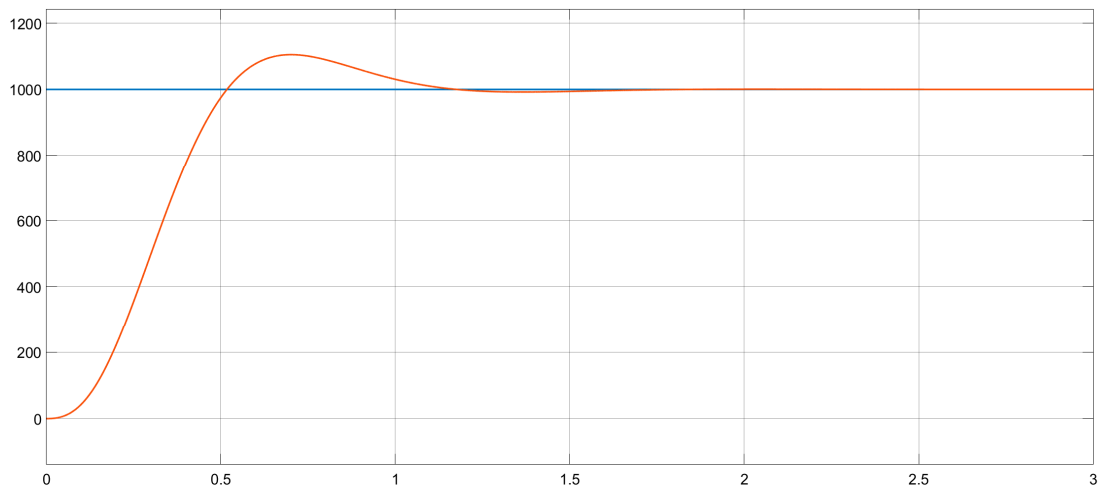


Figure 12. Step Response of the ADRC Speed Loop.

In the speed loop: $k_p = 15$, $\omega_o = 165$. In the position loop: $k_p = 2.2$, $\omega_o = 40$.

Its position loop is shown in Figure 13, and its position step response is shown in Figure 14.

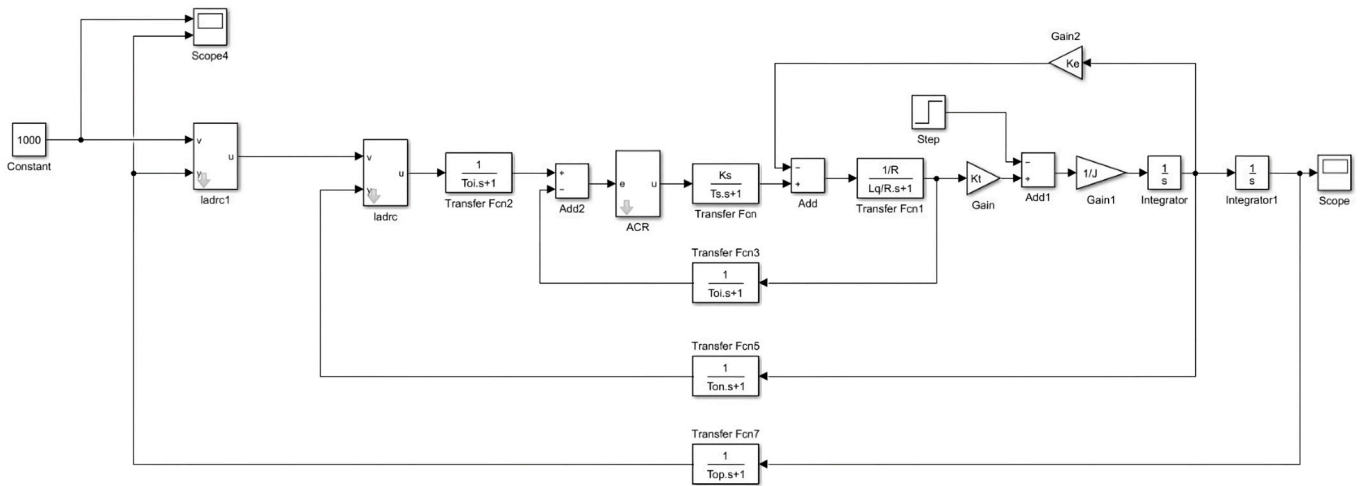


Figure 13. Structure Diagram of the ADRC Position Loop Simulation.

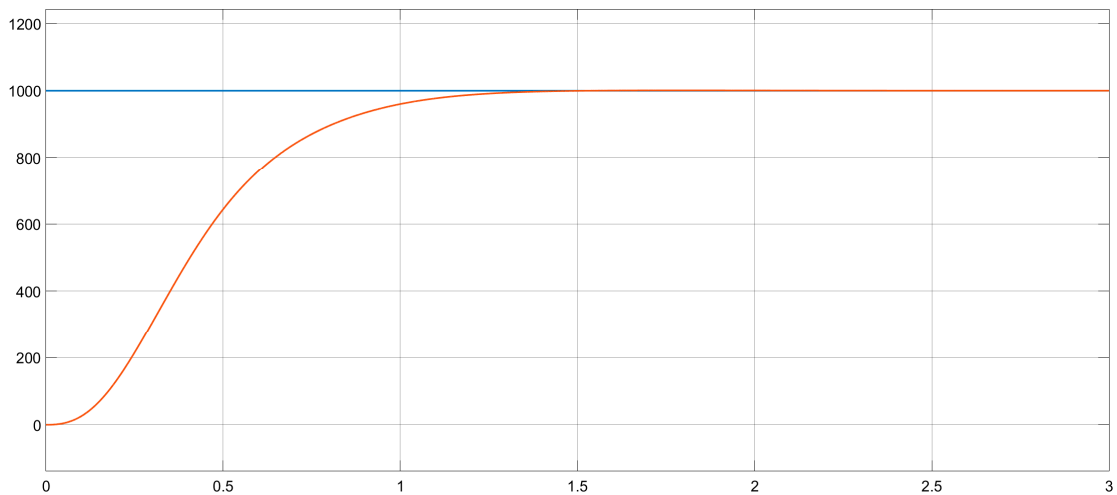


Figure 14. Step Response of the ADRC Position Loop.

3. Results

The EMA test bench is mainly composed of four parts: the base and accessories of the test bench, the EMA and its controller, the sensing and data acquisition system and the power supply system. It is shown in Figure 15.



Figure 15. Test bench system.

The EMA is composed of Kollmorgen's EMA and EXLAR's planetary roller screw mechanism (PRSM). The main parameters of PMSM are: the rated voltage is 220 V, the rated speed is 5000 rpm, the rated power is 0.75 kW, the impedance is 5.3Ω , the quadrature axis inductance is 11 mH, the motor rotational inertia is $1.29 \text{ kg}\cdot\text{cm}^2$, the torque constant is 5.2 N·m/A and the back electromotive force constant is 0.01 V/rpm. The lead of the PRSM is 0.2 inches. The motor controller is the AKD-P00606 drive controller of Kollmorgen, with continuous output power up to 2 kW.

The sensing and data acquisition system consists of a force sensor module, displacement sensor module and data acquisition card. The sensor is used to measure the tension and pressure load of the EMA, and the H3-C3 force sensor of AVIC is adopted. The displacement sensor module is used to measure the output displacement of EMA, and the universal KTC pull rod series linear displacement sensor is adopted. The data acquisition card uses NI's PCI6221 (68 pin), which has 16 analog inputs, 2 analog outputs and 24 digital inputs and outputs. ADC precision is 16 bits, and the maximum sampling rate is 250 kS/s.

The parameter of position loop P regulator in the test is 0.3. The parameters of position loop ADRC controller are $b_0 = 0.1$, $w_0 = 120$, $k_p = 2.5$ and $a = 0.7$.

In the graph, the ordinate unit is mm, and the time unit is 0.2 s.

3.1. Load Step Test

The test method is: the output end of EMA has a load of 50 kg, and the system is powered on. The upper computer gives a step displacement instruction, and the amplitudes are set to 20 mm and 40 mm respectively. The feedback signal of the displacement sensor is read. The 20 mm step test result is shown in Figure 16, and the 40 mm step test result is shown in Figure 17.

The average adjustment time of PID load step of 20 mm is 16.9 s, the average overshoot is 0.37 mm and the average rise time is 14.4 s. The average adjustment time of PID load step 40 mm is 18.6 s, the average overshoot is 0.36 mm and the average rise time is 15.7 s.

The average adjustment time of ADRC load step of 20 mm is 12.4 s, the average overshoot is 0.05 mm and the average rise time is 10.8 s. The average adjustment time of ADRC load step 40 mm is 15.3 s, the average overshoot is 0.1 mm and the average rise time is 13.2 s.

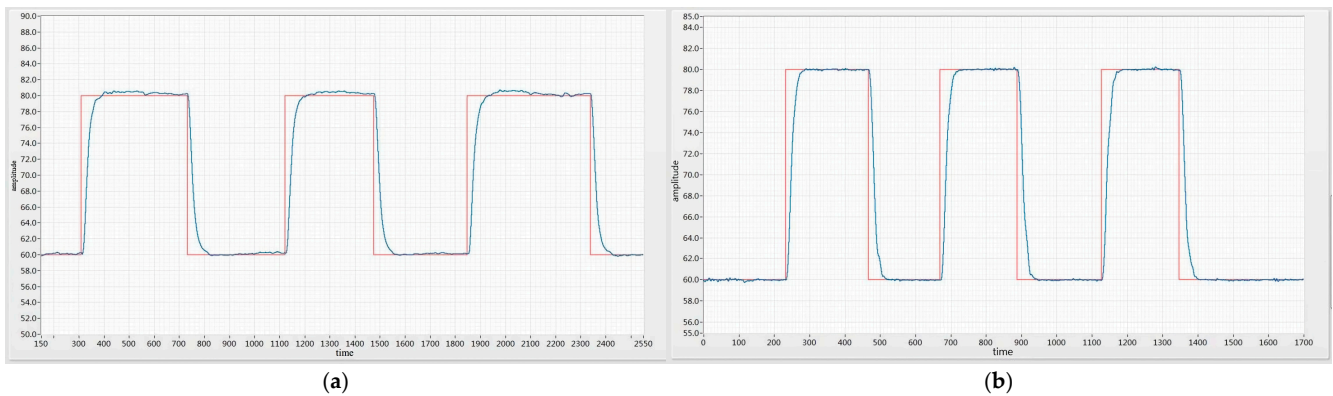


Figure 16. (a) PID load 20 mm step response; (b) ADRC load 20 mm step response.

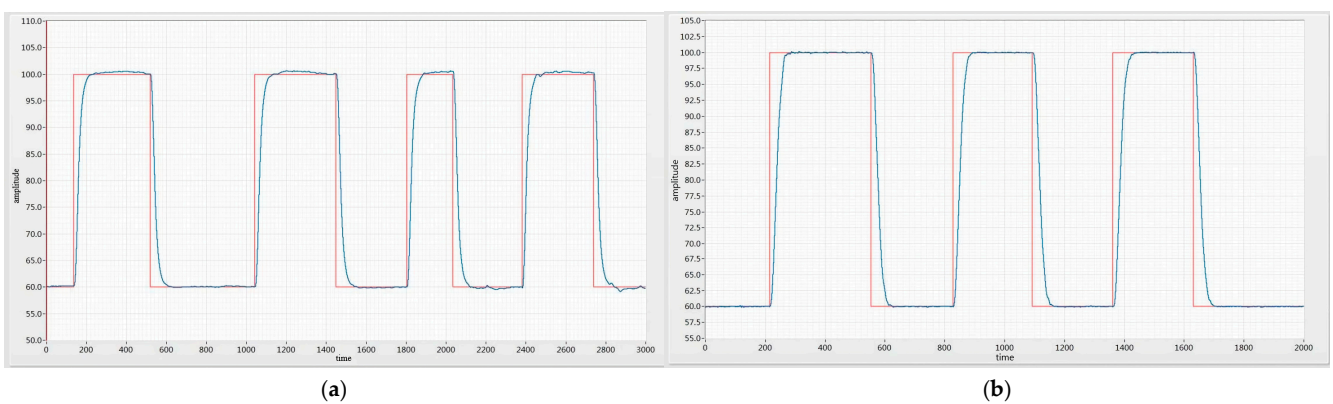


Figure 17. (a) PID load 40 mm step response; (b) ADRC load 40 mm step response.

3.2. Load Disturbance Test

The test method is: the EMA is empty, the system is powered on and the upper computer gives a step displacement instruction. After the displacement is stable, it is suddenly loaded with a load of 50 kg, and the feedback signal of the displacement sensor is read. The 50 kg load disturbance test result is shown in Figure 18.

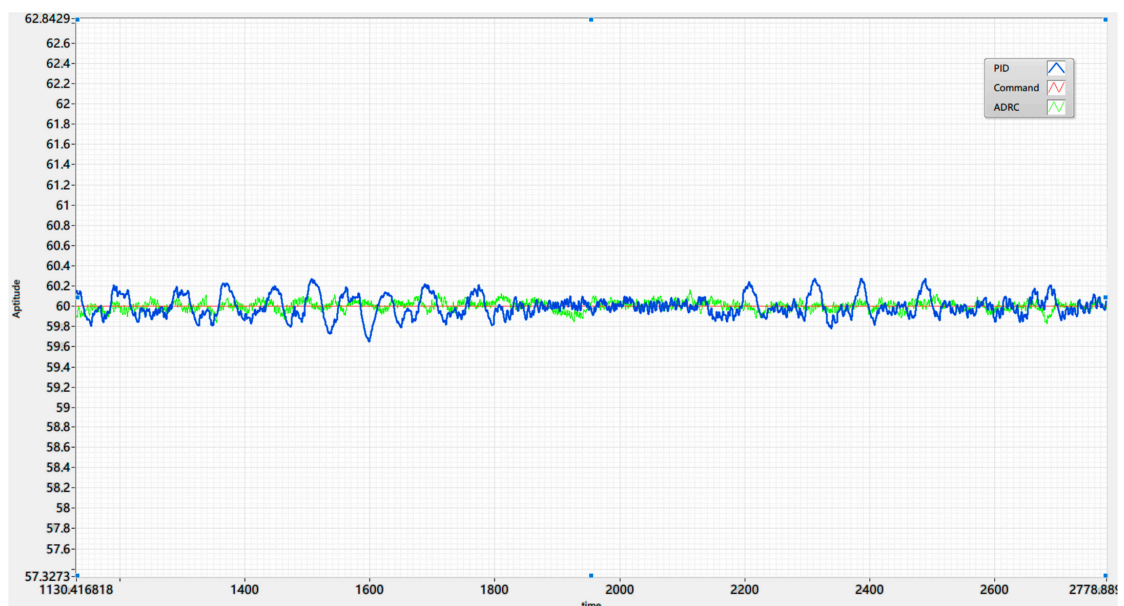


Figure 18. PID 50 kg load disturbance and ADRC 50 kg load disturbance.

The average deviation of the PID load disturbance is 1.33 mm, and the average adjustment time is 28.7 s; the average deviation value of ADRC load disturbance is 0.43 mm, and the average adjustment time is 4.7 s.

4. Discussion

In this paper, the theory, simulation and experimental research of EMA control based on the ADRC method are carried out, and some results have been achieved. However, due to the limitations of the test conditions and personal knowledge levels, there are still some deficiencies. In the future, further research will be carried out that takes into account the following aspects:

1. In the aspect of mathematical modeling, the nonlinear factors such as the clearance and friction of the mechanical system are simplified, and the model is not accurate enough, which needs further improvement;
2. In terms of the calculation method, the discretization method adopted is the Euler method. The approximate accuracy is not high enough, and it is easy to produce a high-frequency tremor. A better discretization method can be adopted;
3. In the system test, the output of the sensor is analog, which is easily affected by noise. The digital sensor can be used to improve the measurement accuracy. The loading mode of the load also needs to be improved.

5. Conclusions

In this paper, an ADRC method with an improved ESO is proposed to design the cascade controller of EMA based on PMSM. The mathematical model of PMSM in a two-phase rotating coordinate system is established, then it is decoupled by an $i_d = 0$ current control method to realize the vector control of the motor. In a three closed-loop vector control system, a PID controller including current loop, speed loop and position loop is designed. The filter link and system are modeled as a whole, and an improved ESO is constructed. On this basis, the ADRC controller of the speed loop and position loop of PMSM is designed and simulated based on Simulink. Based on the physical test platform, a load step test and load disturbance test of ADRC are completed. The results show that ADRC has good static and dynamic performance, which has a good guiding role for engineering practice.

Author Contributions: Q.F., Y.Z., Y.W. and H.H. were in charge of the whole trial; Q.F. wrote the manuscript; C.Z. and S.M. assisted with sampling and laboratory analyses. All authors have read and agreed to the published version of the manuscript.

Funding: This research was funded by Northwestern Polytechnical University Industry Key Technology Research Fund Project, grant No. HXGJXM202205.

Institutional Review Board Statement: Not applicable.

Informed Consent Statement: Not applicable.

Data Availability Statement: Data sharing is not applicable.

Conflicts of Interest: The authors declare no conflict of interest.

References

1. Wang, F.; Liu, E.; Wang, R.; Zhang, W.; Yang, Y. An approach to improve active disturbance rejection control. *Int. J. Control* **2020**, *93*, 1063–1073. [[CrossRef](#)]
2. Fu, C.; Tan, W. Analysis and tuning of reduced-order active disturbance rejection control. *J. Frankl. Inst.* **2021**, *358*, 339–362. [[CrossRef](#)]
3. Feng, H.; Guo, B. Active disturbance rejection control: Old and new results. *Annu. Rev. Control* **2017**, *44*, 238–248. [[CrossRef](#)]
4. Patelski, R.; Dutkiewicz, P. On the stability of ADRC for manipulators with modelling uncertainties. *ISA Trans.* **2020**, *102*, 295–303. [[CrossRef](#)] [[PubMed](#)]
5. Fu, C.; Tan, W. Control of unstable processes with time delays via ADRC. *ISA Trans.* **2017**, *71*, 530–541. [[CrossRef](#)] [[PubMed](#)]

6. Boldea, I.; Tutelea, L.N.; Parsa, L.; Dorrell, D. Automotive Electric Propulsion Systems with Reduced or No Permanent Magnets: An Overview. *IEEE Trans. Ind. Electron.* **2014**, *61*, 5696–5711. [[CrossRef](#)]
7. Zhou, C. Research on EMA Digital Servo Control System. Master's Thesis, Nanjing University of Aeronautics and Astronautics, Nanjing, China, 2013.
8. Ma, Y. Research and Implementation of Control Strategy for EMA Servo Drive System. Master's Thesis, Nanjing University of Aeronautics and Astronautics, Nanjing, China, 2018.
9. Ruiz-Carcel, C.; Starr, A. Data-Based Detection and Diagnosis of Faults in Linear Actuators. *IEEE Trans. Instrum. Meas.* **2018**, *67*, 2035–2047. [[CrossRef](#)]
10. Sun, B.; Gao, Z. A DSP-based active disturbance rejection control design for a 1-kW H-bridge DC-DC power converter. *IEEE Trans. Ind. Electron.* **2005**, *52*, 1271–1277. [[CrossRef](#)]
11. Gao, Z. Active Disturbance Rejection Control: A paradigm shift in feedback control system design. In Proceedings of the American Control Conference, Minneapolis, MN, USA, 14–16 June 2006.
12. Qing, Z.; Gao, Z. On Practical Applications of Active Disturbance Rejection Control. In Proceedings of the Chinese Control conference, Beijing, China, 29–31 July 2010.
13. Zheng, Q.; Gao, L.; Gao, Z. On Validation of Extended State Observer through Analysis and Experimentation. *J. Dyn. Syst. Meas. Control* **2012**, *134*, 024505. [[CrossRef](#)]
14. Shi, Z.; Zhang, P.; Lin, J.; Ding, H. Permanent Magnet Synchronous Motor Speed Control Based on Improved Active Disturbance Rejection Control. *Actuators* **2021**, *10*, 147. [[CrossRef](#)]
15. Zuo, Y.; Ge, X.; Zheng, Y.; Chen, Y.; Wang, H.; Woldegiorgis, A.T. An Adaptive Active Disturbance Rejection Control Strategy for Speed-Sensorless Induction Motor Drives. *IEEE Trans. Transp. Electrif.* **2022**, *8*, 3336–3348. [[CrossRef](#)]
16. Alonge, F.; Cirrincione, M.; D'Ippolito, F.; Pucci, M.; Sferlazza, A. Active disturbance rejection control of linear induction motor. *IEEE Trans. Ind. Appl.* **2017**, *53*, 4460–4471. [[CrossRef](#)]
17. Sira-Ramírez, H.; Linares-Flores, J.; García-Rodríguez, C.; Contreras-Ordaz, M.A. On the control of the permanent magnet synchronous motor: An active disturbance rejection control approach. *IEEE Trans. Control. Syst. Technol.* **2014**, *22*, 2056–2063. [[CrossRef](#)]
18. Alonge, F.; Cirrincione, M.; D'Ippolito, F.; Pucci, M.; Sferlazza, A. Robust active disturbance rejection control of induction motor systems based on additional sliding-mode component. *IEEE Trans. Ind. Electron.* **2017**, *64*, 5608–5621. [[CrossRef](#)]
19. Kato, T.; Xu, Y.; Tanaka, T.; Shimazaki, K. Force control for ultraprecision hybrid electric-pneumatic vertical-positioning device. *Inter-Natl. J. Hydromechatronics* **2021**, *4*, 185–201. [[CrossRef](#)]
20. Togawa, T.; Tachibana, T.; Tanaka, Y.; Peng, J. Hydro-disk-type of electrorheological brakes for small mobile robots. *Int. J. Hydromechatronics* **2021**, *4*, 99–115. [[CrossRef](#)]
21. Yoo, D.; Yau, S.T.; Gao, Z. Optimal fast tracking observer bandwidth of the linear extended state observer. *Int. J. Control* **2007**, *80*, 102–111. [[CrossRef](#)]
22. Yoo, D.; Yau, S.T.; Gao, Z. On Convergence of the Linear Extended State Observer. In Proceedings of the 2006 IEEE Conference on Computer Aided Control System Design, 2006 IEEE International Conference on Control Applications, 2006 IEEE International Symposium on Intelligent Control, Munich, Germany, 4–6 October 2006.
23. Colgren, R.; Frye, M. The design and integration of electromechanical actuators within the U-2S aircraft. In Proceedings of the Guidance, Navigation, and Control Conference and Exhibit, Beijing, China, 22 August 2012.
24. Chen, G.; Zeng, M.; Wei, L. Overview of sensorless permanent magnet synchronous motor vector control system. *Weite Mot.* **2011**, *39*, 64–67.
25. Zhu, B. *Introduction to Active Disturbance Rejection Control*; Beijing University of Aeronautics and Astronautics Press: Beijing, China, 2017.

Disclaimer/Publisher's Note: The statements, opinions and data contained in all publications are solely those of the individual author(s) and contributor(s) and not of MDPI and/or the editor(s). MDPI and/or the editor(s) disclaim responsibility for any injury to people or property resulting from any ideas, methods, instructions or products referred to in the content.